

Do LLMs and VLMs Share Neurons for Inference? Evidence and Mechanisms of Cross-Modal Transfer

Chenhang Cui¹ An Zhang^{2*} Yuxin Chen¹ Gelei Deng³ Jingnan Zheng¹
 Zhenkai Liang¹ Xiang Wang² Tat-Seng Chua¹

¹National University of Singapore, Singapore

²University of Science and Technology of China, Hefei, China

³Nanyang Technological University, Singapore

Abstract

*Large vision-language models (LVLMs) have rapidly advanced across various domains, yet they still lag behind strong text-only large language models (LLMs) on tasks that require multi-step inference and compositional decision-making. Motivated by their shared transformer architectures, we investigate whether the two model families rely on common internal computation for such inference. At the neuron level, we uncover a surprisingly large overlap: more than half of the top-activated units during multi-step inference are shared between representative LLMs and LVLMs, revealing a modality-invariant inference subspace. Through causal probing via activation amplification, we further show that these shared neurons encode consistent and interpretable concept-level effects, demonstrating their functional contribution to inference. Building on this insight, we propose **Shared Neuron Low-Rank Fusion (SNRF)**, a parameter-efficient framework that transfers mature inference circuitry from LLMs to LVLMs. SNRF profiles cross-model activations to identify shared neurons, computes a low-rank approximation of inter-model weight differences, and injects these updates selectively within the shared-neuron subspace. This mechanism strengthens multimodal inference performance with minimal parameter changes and requires no large-scale multimodal fine-tuning. Across diverse mathematics and perception benchmarks, SNRF consistently enhances LVLM inference performance while preserving perceptual capabilities. Our results demonstrate that shared neurons form an interpretable bridge between LLMs and LVLMs, enabling low-cost transfer of inference ability into multimodal models. Our code is available at <https://github.com/chenhangcuisg-code/Do-LLMs->*

VLMs-Share-Neurons.

1. Introduction

Large vision-language models (LVLMs) have achieved rapid progress on various tasks such as captioning [23], grounding [34], recommendation [27], and interaction [61], yet—as repeatedly observed in recent studies [18, 21, 56]—their general multi-step inference ability remains substantially weaker than that of strong text-only large language models (LLMs). A prevailing approach to close this gap has been to scale LVLMs with more multimodal data and larger size [3, 6, 8]. However, scaling alone faces persistent obstacles: the amount of paired image-rationale data is still limited compared to the vast text corpora [1, 2, 57], and it remains unclear how general abilities acquired by LLMs should transfer to multimodal settings. These limitations raise a natural question: **Can we leverage the relatively mature capabilities of LLMs to enhance LVLMs at a relatively low cost?**

Prior studies show that models sharing similar architectures often exhibit consistent internal behavior [7, 43, 51]. Motivated by this, we investigate whether LLMs and LVLMs display comparable consistency in inference. We perform neuron-level activation profiling [5, 7] to identify the units that activate most strongly during inference tasks. Across distinct LLM and LVLM families (e.g., Qwen2.5-Math [52] vs. Qwen2.5-VL [3]; Idefics3 [20] vs. Deepseek-LLaMA3 [17]), we find that more than half of the top-activated neurons overlap. This nontrivial consistency suggests that, despite differences in modality and training corpora, these models surprisingly converge on similar internal pathways for inference. To further probe this phenomenon, we conduct an amplification-based analysis: boosting the activations of the overlapped neurons and measuring the resulting changes in model outputs. This reveals

*Corresponding author.

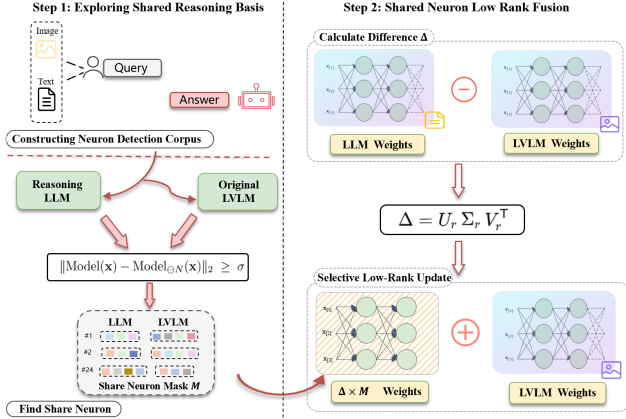


Figure 1. Overview of the proposed Shared Neuron Low-Rank Fusion (SNRF) framework. SNRF first performs neuron-level activation profiling to identify neurons that are consistently co-activated during inference across an LLM and an LVLM. The intersection of these units forms a shared neuron subspace, which is reused and amplified through low-rank adapters.

that the shared neurons encode coherent, functional concepts—many of them math-related—and that amplifying these units systematically strengthens inference behaviors. These findings clearly indicate that LLMs and LVLMs share a transferable neuron subspace. Building on this observation, leveraging these neurons provides an efficient pathway for transferring relatively mature inference capabilities of LLMs into multimodal models.

Motivated by this insight, we propose **Shared Neuron Low-Rank Fusion (SNRF)**, a parameter-efficient framework that transfers inference circuitry from an LLM to an LVLM by explicitly reusing the subset of neurons that both models activate during inference. The overall framework is shown in Figure 1. SNRF first identifies a set of *shared neurons* by profiling cross-model activations on inference prompts and then computes a low-rank approximation of the inter-model weight difference. The low-rank update is projected onto the shared-neuron subspace, injecting compact inference signals while preserving the LVLM’s perceptual pathways. SNRF enables efficient transfer without large-scale multimodal training. SNRF is extensively evaluated on diverse multimodal benchmarks spanning science QA, mathematics, and perception tasks. As shown in Figure 2, SNRF consistently improves LVLM performance while maintaining its original visual and perceptual capabilities.

Our contributions are threefold. First, we provide an empirical finding that LLMs and LVLMs exhibit substantial overlap among their top-activated neurons during language inference, suggesting the existence of a shared neuron subspace across modalities. Second, we introduce an amplification-based neuron analysis that enhances specific activations to reveal their functional concepts and causal

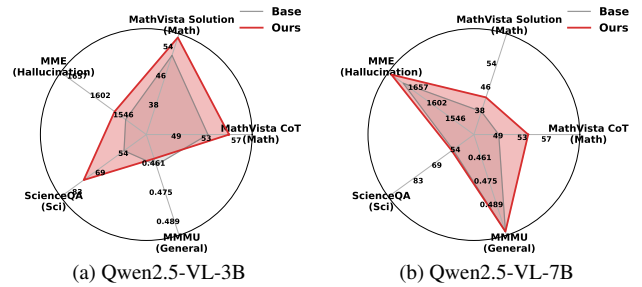


Figure 2. Comparison of Base and our method across five multimodal benchmarks. Our method consistently enhances mathematical performance while maintaining comparable robustness on general metrics.

influence on model outputs, enabling concept-level interpretation of inference units. Third, we propose SNRF, a parameter-efficient framework that aligns and reuses consistently activated neurons to transfer mature text inference into LVLMs with minimal additional cost.

2. Related Work

Large Vision and Language Models. Modern vision-language models increasingly adopt a pretrained LLM as the text decoder, paired with a vision encoder and a lightweight projector. This shift—from contrastive encoder-decoder frameworks (e.g., CLIP-style contrastive pretraining [37, 58]) to LLM-centric designs—has enabled stronger transfer and significantly easier scaling. Recent models (e.g., Qwen2.5-VL [3], LLaVA-OneVision [22]) broaden inputs from single images to multi-image sequences, while a unified architecture and tighter cross-modal attention further improve fusion quality. Beyond visual instruction tuning [25, 60], multimodal alignment increasingly adopts reinforcement learning (RL)-based preference optimization [42, 45] and verifiable-reward paradigms [28, 47] to enhance stepwise fidelity, safety, and calibration. For inference, chain-of-thought has been extended to incorporate visual grounding [40, 59], and tool-augmented pipelines [35] dispatch subproblems to external vision modules or generated code to solve complex queries. Despite these recent architectural and alignment advances, LVLMs still lag behind strong text-only LLMs in compositional inference under visual contexts. Benchmarks such as Exams-V [11] and MMMU-Pro [56] consistently reveal substantial gaps in faithfulness, robustness, and numerical accuracy, suggesting that scaling and alignment alone do not fully close the gap.

Interpreting Neurons and Features in Models. Early work showed that single units in sequence models can represent clear meanings: for example, a single “sentiment neuron” appeared in a character-level review generator [36],

and manual inspections of character RNNs found neurons that track quotes, brackets, and URLs [19]. Subsequent studies identified “knowledge neurons” in Transformer-based language models whose activations directly influence cloze completions of factual entities [10]. This complements evidence that MLP layers work like key-value memories that store word and concept associations [16]. Since many neurons are not tied to just one concept, some work describes their behavior as combinations of multiple features [31]. At larger scales, some techniques use strong LMs to generate natural-language hypotheses about thousands of neurons and then score them for accuracy [33]. For vision-language models (LVLMs), CLIP revealed “multi-modal neurons” that respond to both text and images for abstract ideas (e.g., celebrities, symbols) [32]. Extending “knowledge neurons” to LVLMs, a two-stage filtering method found units linked to world knowledge in MiniGPT-4 and enabled targeted edits during image captioning [39]. Other recent studies also explore safety neurons that affect alignment-related refusal or harmful outputs [5], and multi-lingual neurons that hold language-specific competence and can steer which language the model uses [7]. Overall, these studies suggest that neurons provide a useful basis for understanding the abilities of modern models. However, no prior work has investigated whether inference-related neurons are shared across LLMs and LVLMs, nor how such shared circuitry can be leveraged for cross-model transfer—a gap our work aims to fill.

3. Preliminary

Transformer-based language models. A Transformer block consists of a multi-head attention (MHA) module and a feed-forward network (FFN or MLP), both operating on the residual stream. Given an input sequence $w = \langle w_0, \dots, w_t \rangle$, token embeddings h_i are produced by W_E and accumulated in the residual stream. Each block then refines this stream (layer normalization omitted):

$$h_i^{\ell+1} = h_i^\ell + \text{MHA}^\ell(h_i^\ell) + \text{MLP}^\ell(h_i^\ell + \text{MHA}^\ell(h_i^\ell)). \quad (1)$$

Feed-forward neurons. In modern Transformers, the feed-forward network (FFN), or multi-layer perceptron (MLP), can be expressed as

$$\text{MLP}(x) = W_{\text{down}}^\top \sigma(W_{\text{up}}x), \quad (2)$$

where $W_{\text{up}}, W_{\text{down}} \in \mathbb{R}^{d_m \times d}$. Here W_{up} projects the residual stream into a higher-dimensional space (`fw.d.up`), producing intermediate activations. A non-linear activation $\sigma(\cdot)$ is then applied, and W_{down} projects the result back to the model dimension d (`fw.d.down`).

Attention neurons. The multi-head attention module computes token interactions via four projection matrices:

$$Q = W_Q h, \quad K = W_K h, \quad V = W_V h, \quad (3)$$

where $W_Q, W_K, W_V \in \mathbb{R}^{d \times d}$ are the query, key, and value, respectively. Analogous to the MLP case, each row or column of these matrices may be regarded as a *neuron*: - `attn.q`: query neurons that encode how tokens *ask for* information; - `attn.k`: key neurons that encode how tokens *offer* information; - `attn.v`: value neurons that carry the content to be propagated;

Neuron Types Used in Our Work. In this work, we analyze these neurons in both LLMs and LVLMs, focusing on their roles in inference. This unified view enables us to compare the neurons `{attn.q, attn.k, attn.v, fwd.up, fwd.down}` and to investigate whether shared inference circuitry emerges across modalities.

4. Exploring Shared inference Basis

4.1. Identifying Important Neurons in LLMs and LVLMs

Constructing Neuron Detection Corpus c . To identify neurons that are important for inference in both LLMs and LVLMs, we define a neuron detection corpus c as a set of m probe inputs $c = \{\mathbf{x}_i\}_{i=1}^m$, where each \mathbf{x}_i concatenates a problem with the model’s own inference output to elicit genuine inference activations. We explicitly study two categories of base models: *text models* and *vision-language (VL) models*. In the text-only pipeline (GSM8K [9]), a text model M_0^{text} generates a rationale r_i and prediction \hat{a}_i for problem q_i , and we build $\mathbf{x}_i^{Q+A} = [\text{INST}]\|q_i\|[\text{SEP}]\|(r_i, \hat{a}_i)$. The token `INST` specifies the instruction prefix that standardizes the output format, and `SEP` is a separator token that marks the boundary between the original problem and the model-generated inference. The operator “`||`” represents sequence concatenation. In the multimodal pipeline (Geo3K [29]), a frozen VL model M_0^{vl} consumes both the problem text q_i and image I_i , where the image is encoded into visual tokens $v_i = \phi(I_i)$, yielding $\mathbf{x}_i^{V+L} = [\text{INST}]\|v_i\|q_i\|[\text{SEP}]\|(r_i, \hat{a}_i)$. This separation allows us to compare inference neurons activated in textual inference versus those engaged in multimodal inference.

Activation Profiling for Identifying inference Neurons.

We use activation profiling to identify inference neurons, defined as neurons that are consistently activated when processing inputs from inference tasks. Here, a neuron refers to a single row or column within the model’s parameter matrices. Building on prior work in identifying important neurons in neural networks [5, 14, 46], we consider a neuron

to be activated if its removal leads to a significant change in the resulting embedding. Formally, given an input sequence \mathbf{x} from context c , a neuron N is considered activated if

$$\|\text{Model}(\mathbf{x}) - \text{Model}_{\ominus N}(\mathbf{x})\|_2 \geq \sigma, \quad (4)$$

where $\text{Model}(\mathbf{x})$ denotes the output embedding when processing \mathbf{x} , and $\text{Model}_{\ominus N}(\mathbf{x})$ denotes the output when neuron N is deactivated by zeroing the parameters that produce or consume it. The threshold σ specifies the minimum magnitude of change required to consider a neuron activated. Context-related neurons for a specific context c are then

$$\mathcal{N}_{\text{ctx}}^c := \left\{ N \in \text{Model} \mid \|\text{Model}(\mathbf{x}) - \text{Model}_{\ominus N}(\mathbf{x})\|_2 \geq \sigma, \forall \mathbf{x} \in c \right\}. \quad (5)$$

We apply Eq. 4-5 separately to the text model M_0^{text} and the VL model M_0^{vl} .

Inference Basis Neurons. Our goal is to identify neurons that consistently support inference across both **text** and **vision-language (VL)** models. Let $\mathcal{C}_{\text{text}}$ and \mathcal{C}_{vl} denote the sets of contexts from the text-only and multimodal pipelines, respectively. Using Eq. 5, compute context-related sets for each model, $\mathcal{N}_{\text{ctx}}^c(M_0^{\text{text}})$ and $\mathcal{N}_{\text{ctx}}^c(M_0^{\text{vl}})$, restricted to neurons with one-to-one correspondence in the shared language backbone. We define the *inference Basis (shared) neurons* as

$$\mathcal{N}_{\text{shared}} := \left(\bigcap_{c \in \mathcal{C}_{\text{text}}} \mathcal{N}_{\text{ctx}}^c(M_0^{\text{text}}) \right) \cap \left(\bigcap_{c \in \mathcal{C}_{\text{vl}}} \mathcal{N}_{\text{ctx}}^c(M_0^{\text{vl}}) \right). \quad (6)$$

This definition explicitly measures neurons that support inference across both model classes, while separating those specialized to text-only or multimodal settings.

Neuron-Concept Validation via Amplification. To more clearly assess the functional role of each neuron, we amplify its activation during the forward pass:

$$N \leftarrow \lambda \cdot N, N \in \mathcal{N}_{\text{shared}}, \quad (7)$$

where λ denotes the amplification factor. For each token t , we directly measure its frequency under amplified runs:

$$F_\lambda(t) = \sum_{\mathbf{x} \in c} \sum_j \mathbb{1}[y_j^{\oplus \lambda N} = t \mid x^Q, y_{< j}], \quad (8)$$

where $y_j^{\oplus \lambda N}$ denotes the token generated at position j when neuron N is amplified.

4.2. Findings of Shared Inference Basis

In this section, we report three findings that together illuminate the shared inference mechanisms underlying diverse model families.

Finding 1

Different series of VL models and their corresponding text-math models share a large number of neurons on inference tasks.

Strong overlap. Across multiple LLM/LVLM families (e.g., Qwen2.5-VL-7B [3] vs. Qwen2.5-Math-7B [52]; Intern2.5-VL-3B [8] vs. Qwen2.5-GRPO-3B [49]; LLaVA-Next-8B [26] vs. LLaMA3-DeepSeek-8b [17]), we observe a substantial intersection between the sets of neurons activated by inference inputs. As shown in Figure 3, the Qwen2.5-7B-Math and Qwen2.5-7B-VL share 4,703 neurons out of a union of 6,312 (74.5% of the union), with only 667 (10.6%) and 942 (14.9%) neurons remaining model-specific. Similar levels of overlap are also observed in the Idifics3-8B. Interestingly, we further find that even models without identical language backbones still exhibit a non-negligible proportion of shared neurons, suggesting the existence of universal inference units that transcend architectural differences. See details in Appendix C.1.

This magnitude of overlap is consistently seen across other model pairs we tested (details in Appendix), indicating that a nontrivial portion of the inference circuitry is reused between text-only and multimodal models despite their different training signals.

Where the shared neurons live. We next examine how the shared neurons distribute across layers and modules. As shown in Figure 4, the shared neurons in Qwen2.5-VL-7B and Qwen2.5-Math-7B are clearly concentrated in the `attn.k` matrices across nearly all layers, with a secondary presence in `attn.v`. Additionally, distinct clustering emerges in the early layers (e.g., before layer 6), and again in later layers (after layer 20). Further examples are provided in Appendix C.1.

Finding 2

Shared inference basis plays an important role in a model’s performance on inference tasks.

We evaluate the *causal* role of shared neurons ($\mathcal{N}_{\text{shared}}$; Eq. 6) by (i) **Deact**—zeroing the parameters that produce/consume only neurons in $\mathcal{N}_{\text{shared}}$; and (ii) **Random Deact**—ablating the *same number* of neurons sampled at random from the same layer-module budget.

Table 5 summarizes the effect on accuracy in Math-Vista [30], a comprehensive benchmark for mathematical

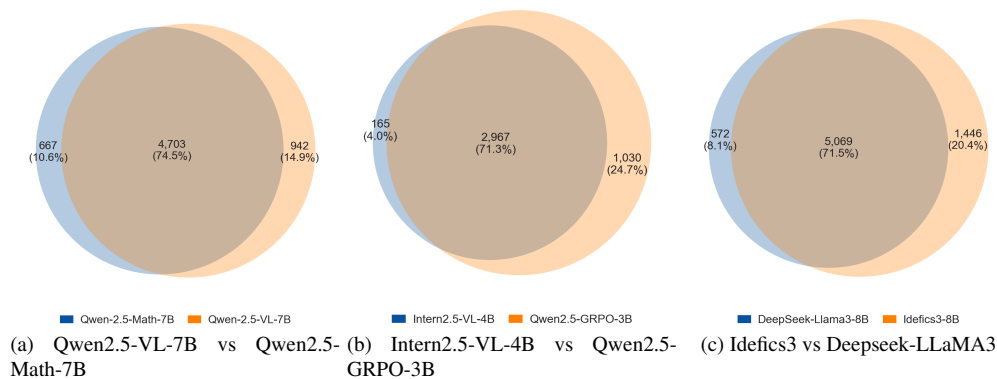


Figure 3. Overlap of activated neurons across different LVLm families.

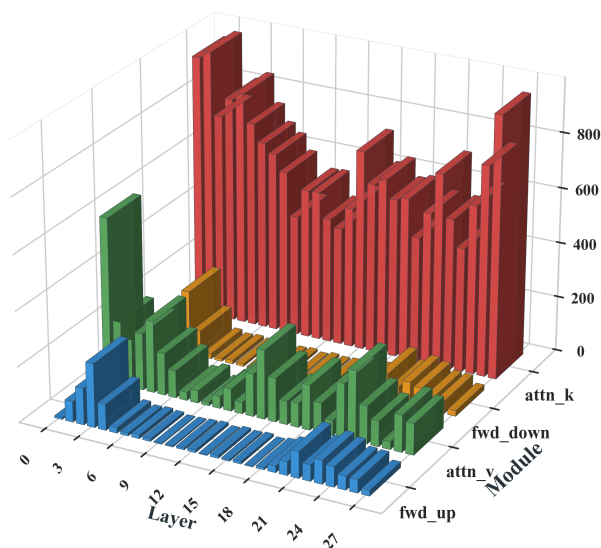


Figure 4. Distribution of shared neurons across layers and modules in Qwen2.5-VL-7B and Qwen2.5-Math-7B. A clear concentration appears in `attn.k`, with secondary presence in `attn.v`. Clustering is most evident in early layers and later layers.

inference in multimodal large language models. Across three LVLms, deactivating the shared neurons collapses performance to **0.0**, whereas random ablations of equal size lead to notably smaller drops. Parallel trends appear across additional benchmarks (see Appendix C.2), indicating that the shared neurons are *both necessary and specific* to inference. The dramatic failure under **Deact**—in sharp contrast to the partial degradation under **Random Deact**—shows that the *shared inference basis* encodes functionally indispensable circuitry for multimodal inference rather than generic capacity or redundant pathways. Further results on

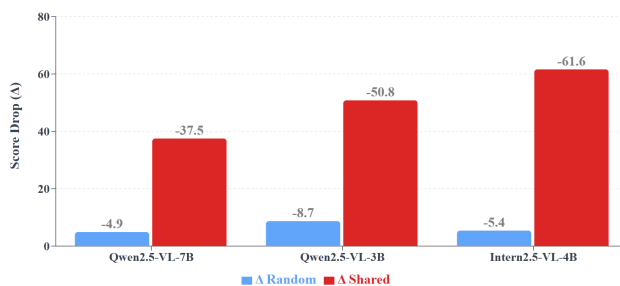


Figure 5. Effect of ablating shared neurons on MATHVISTA. Arrows indicate higher is better.

a wider suite of tasks (Appendix C.2) reinforce this pattern, underscoring the centrality of these shared neurons to robust inference behavior.

Finding 3

A large portion of shared neurons are linked to math inference.

Using our amplification method (§3), we find shared neurons in both LLMs and LVLms that show clear activation on mathematical concepts. To better illustrate this, we build word clouds from the amplified generations of Qwen2.5-Math-7B, where token substrings are mapped back to their original text. Word size shows activation frequency, making the main math tendencies of each neuron visible. As shown in Figure 6, different neurons are sensitive to different parts of math inference. For example, neuron `fwd.up.L14.N12953` activates on algebra and arithmetic tokens (e.g., numbers, “met,”), while neuron `fwd.down.L10.N1889` responds to geometry and measurement concepts (e.g., “cube,” “square,” “round”). These patterns suggest that some neurons specialize in certain types of mathematical knowledge. This finding shows

the original model? (2) How does our method perform compared to other baselines? (3) How well does our method generalize to other parameter-merging techniques?

6.1. Setup

Backbones. Unless otherwise noted, we evaluate LVLMS at small/medium scales (3B–8B) built on two language backbones: (i) **Llama 3**—*Idefics3-8B-LLaMA3* [20] and *LLaVA-Next-8B* [26], where the corresponding text model used for merging is *DeepSeek-LLaMA3* [17]; (ii) **Qwen2.5**—We evaluate *Qwen2.5-VL-3B*, *Qwen2.5-VL-7B* [3], and *Intern2.5-VL-4B* [8]. For parameter merging, *Qwen2.5-VL-7B* is paired with *Qwen2.5-Math* [52], whereas *Intern2.5-VL-4B* and *Qwen2.5-VL-3B* are paired with the text backbone *Qwen3B-GRPO* [49]. Each model uses its official vision encoder as released by the authors. Exact model and checkpoints are listed in Appendix D.1.

Benchmarks. We include *MathVista* [30] for visual mathematical inference, *MME* [15] for broad perception and cognition, *POPE* [24] for hallucination detection, and *ScienceQA* [38] for multimodal scientific problem solving with explanations. Together, these benchmarks allow us to measure modality alignment, perception→inference competence, and safety/calibration under diverse conditions. We evaluate models on both the original *MMMU* [54] and the more challenging *MMMU-Pro* [55]. *MMMU* evaluates college-level, multi-discipline multimodal understanding, while *MMMU-Pro* introduces harder questions and stricter protocols for more robust cross-domain inference. Full dataset splits, preprocessing details, and license information are provided in Appendix D.2.

Baselines. We compare our approach against a diverse set of publicly available LVLMS baselines at both the 3B and 7B scales. These baselines all involve training strategies designed to enhance inference ability, including supervised fine-tuning and reinforcement learning, including: *Qwen2.5-VL CoT-SFT* (Training via chain of thought supervised finetuning) [13], *Qwen2.5-VL Open-R1-Distill* [44], *VLAA-thinker* [4], *Omlab-VL-Math* [41], *Qwen2.5-VL GRIT* [12]. For our method, we additionally explore merging-based training, which is reported separately. We also experiment with other merging approaches such as linear merge [50], *DARE* [53], and *FRANK* [48] to merge shared neurons of LLMs and LVLMS.

6.2. Results and Analysis.

Comparison with original models. As summarized in Table 1, our selective fusion on shared neurons yields consistent improvements over the original models on *inference-centric* benchmarks while largely preserving perception and

hallucination behavior. On **MathVista**, we observe an average gain of **+2.0** points on *Solution* and **+1.66** on *CoT*, with the largest boosts on *Qwen2.5-VL-3B* (+4.7 *Solution*, +2.6 *CoT*) and *Qwen2.5-VL-7B* (+4.6 *Solution*, +4.5 *CoT*). The *Format* score slightly decreases on average (-0.98), indicating that our method primarily transfers *inference* rather than output formatting; this can be mitigated with a lightweight formatting adapter. On **MMMU/Pro**, the stricter *MMMU-Pro (V)* improves across backbones by **+0.0627** on average, with a notable jump on *Intern2.5-VL-4B* (0.000 → **0.186**). In contrast, *MMMU (val)* remains essentially flat, suggesting that our gains concentrate on harder, verification-style settings rather than inflating validation averages. For **ScienceQA**, where textual inference is prominent, we see sizable improvements (**+7.64** on average): *Qwen2.5-VL-3B* rises by +22.6 and *Idefics3-8B-LLaMA3* by +14.6, supporting our hypothesis that shared neurons encode reusable math/science primitives transferable from text to multimodal contexts. Perception and hallucination metrics remain stable. The aggregate **MME** score increases by **+20.2** on average (e.g., +36 on *LLaVA-Next-8B* and +32 on *Qwen2.5-VL-7B*), while **POPE** is effectively unchanged. This stability is consistent with our design: only neurons empirically identified as *shared inference* units are updated.

Comparison with training baselines. As shown in Figure 7, *Ours (Merge)* is strongest on inference-intensive metrics while preserving perception. At 3B, it leads on **MathVista-Solution** (55.5) and **ScienceQA** (75.1), and stays near SOTA on **MME/POPE** (1559/88.0 vs. 1560/88.3). At 7B, it achieves the best **MMMU-Pro (V)** (0.179 (prev. best 0.1162) and essentially ties **MMMU (val)** (0.503 vs. 0.5033). Compared with the corresponding *Qwen2.5-VL* baselines, **CoT/Solution** improve at both scales (3B: +2.6/+4.7; 7B: +4.5/+4.6). Remaining gaps are mainly on **formatting-heavy** metrics (*MathVista-Format*) and 7B **ScienceQA** versus SFT-specialized models, while perception and hallucination metrics remain stable.

Generalizability of merging strategies. Table 2 evaluates the generalizability of our shared-neuron merge strategy. On *Qwen2.5-VL-7B*, applying *Merge* yields *MMMU-Pro (V)* 0.179 (vs. Linear 0.165, *DARE* 0.125, *FRANK* 0.107) and *MME* 1713, while keeping *MMMU (val)* stable (0.503) and *POPE* stable (86.5); *MathVista* reaches 53.3/68.1/42.1 (*CoT/Format/Solution*). On *Intern2.5-VL-4B*, *Merge* achieves *MathVista* 60.6/65.9/61.3 and *MMMU-Pro (V)* 0.186, with *MMMU (val)* (0.486) and perception metrics (*MME* 1677, *POPE* 90.7) maintained. These results show that merging shared neurons is a generally effective strategy: different merge formulations such as Linear, *DARE*, and *FRANK* can also improve abilities of LVLMS.

Table 1. **Main results of our Shared Neuron Low-Rank Fusion (SNRF) across backbones.** Numbers in parentheses for *Ours* denote absolute deltas vs. the corresponding baseline. Higher is better for all metrics shown.

Model	CoT \uparrow	Format \uparrow	Solution \uparrow	MME \uparrow	POPE \uparrow	ScienceQA \uparrow	MMMU (val) \uparrow	MMMU-Pro (V) \uparrow
Qwen2.5-VL-3B	52.6	61.6	50.8	1535.0	87.2	52.5	0.461	0.018
<i>Ours</i>	55.2 (+2.6)	57.9 (-3.7)	55.5 (+4.7)	1559.0 (+24.0)	88.0 (+0.8)	75.1 (+22.6)	0.458 (-0.003)	0.070 (+0.052)
Qwen2.5-VL-7B	48.8	68.8	37.5	1681.0	86.2	54.5	0.503	0.116
<i>Ours</i>	53.3 (+4.5)	68.1 (-0.7)	42.1 (+4.6)	1713.0 (+32.0)	86.5 (+0.3)	55.4 (+0.9)	0.503 (-0.000)	0.179 (+0.063)
Intern2.5-VL-4B	60.4	65.1	61.6	1670.0	90.8	97.4	0.491	0.000
<i>Ours</i>	60.6 (+0.2)	65.9 (+0.8)	61.3 (-0.3)	1677.0 (+7.0)	90.7 (-0.1)	97.3 (-0.1)	0.486 (-0.005)	0.186 (+0.186)
Idefics3-8B-LLaMA3	50.1	50.4	50.3	1458.0	86.0	25.9	0.423	0.084
<i>Ours</i>	50.4 (+0.3)	49.6 (-0.8)	51.1 (+0.8)	1460.0 (+2.0)	84.9 (-1.1)	40.5 (+14.6)	0.426 (+0.002)	0.097 (+0.013)
LLaVA-Next-8B	35.8	38.6	36.0	1586.0	87.2	74.4	0.410	0.051
<i>Ours</i>	36.5 (+0.7)	38.1 (-0.5)	36.2 (+0.2)	1622.0 (+36.0)	87.5 (+0.3)	74.6 (+0.2)	0.400 (-0.010)	0.051 (+0.000)



Figure 7. Results on MathVista-TestMini (CoT/Format/Solution), MME, POPE, ScienceQA, MMMU (val) and MMMU-Pro (V) for 3B and 7B scales. Note that Qwen2.5-VL-7B-CoT-SFT, Omlab-VL-3B-Math and Qwen2.5-VL-3B-GRIT do not have corresponding 3B and 7B versions, so their results are not reported.

7. Conclusion

This work uncovers a shared neuron subspace between LLMs and LVLMs, showing that many of the most active neurons overlap across modalities and encode causal, concept-level semantics. Leveraging this insight, we introduce **Shared Neuron Low-Rank Fusion (SNRF)**, a parameter-efficient method that transfers mature textual

abilities into LVLMs by selectively aligning and updating these shared neurons. SNRF consistently improves multimodal inference while preserving perception and hallucination performance, outperforming training-based and merging baselines. These findings suggest that LLMs and LVLMs share internal inference circuitry, offering a pathway for cross-domain knowledge transfer—such as from

Table 2. Generalizability of merge strategies. Merging shared neurons—whether by our method or alternative schemes—consistently strengthens verification-style inference (*MMMU-Pro (V)*) while preserving perception and hallucination performance. Our *Ours* achieves the most pronounced verification gains.

Baseline	CoT	Format	Solution	MME	POPE	ScienceQA	MMMU (val)	MMMU-Pro (V)
Qwen2.5-VL-7B	48.8	68.8	37.5	1681.0	86.2	54.5	0.503	0.116
+Linear	52.4	61.3	44.1	1669.0	86.4	56.4	0.450	0.165
+DARE	49.7	65.6	43.2	1677.0	86.3	58.2	0.511	0.125
+FRANK	49.4	68.3	42.7	1667.0	86.6	57.2	0.493	0.107
Intern2.5-VL-4B	60.4	65.1	61.6	1670.0	90.8	97.4	0.491	0.000
+Linear	60.2	65.8	61.8	1670.0	90.8	97.2	0.493	0.209
+DARE	59.7	65.6	63.2	1669.0	90.9	97.4	0.486	0.181
+FRANK	59.2	65.7	61.1	1667.0	86.6	97.3	0.493	0.196

code or math specialists to multimodal models.

References

- [1] Jean-Baptiste Alayrac, Jeff Donahue, Pauline Luc, Antoine Miech, Iain Barr, Yana Hasson, Karel Lenc, Arthur Mensch, Katherine Millican, Malcolm Reynolds, et al. Flamingo: a visual language model for few-shot learning. *Advances in neural information processing systems*, 35:23716–23736, 2022. 1
- [2] Anas Awadalla, Le Xue, Oscar Lo, Manli Shu, Hannah Lee, Etash Guha, Sheng Shen, Mohamed Awadalla, Silvio Savarese, Caiming Xiong, et al. Mint-1t: Scaling open-source multimodal data by 10x: A multimodal dataset with one trillion tokens. *Advances in Neural Information Processing Systems*, 37:36805–36828, 2024. 1
- [3] Shuai Bai, Keqin Chen, Xuejing Liu, Jialin Wang, Wenbin Ge, Sibao Song, Kai Dang, Peng Wang, Shijie Wang, Jun Tang, et al. Qwen2. 5-vl technical report. *arXiv preprint arXiv:2502.13923*, 2025. 1, 2, 4, 7
- [4] Hardy Chen, Haoqin Tu, Fali Wang, Hui Liu, Xianfeng Tang, Xinya Du, Yuyin Zhou, and Cihang Xie. Sft or rl? an early investigation into training rl-like reasoning large vision-language models, 2025. 7
- [5] Jianhui Chen, Xiaozhi Wang, Zijun Yao, Yushi Bai, Lei Hou, and Juanzi Li. Finding safety neurons in large language models. *arXiv preprint arXiv:2406.14144*, 2024. 1, 3, 11
- [6] Xi Chen, Josip Djolonga, Piotr Padlewski, Basil Mustafa, Soravit Changpinyo, Jialin Wu, Carlos Riquelme Ruiz, Sebastian Goodman, Xiao Wang, Yi Tay, et al. Pali-x: On scaling up a multilingual vision and language model. *arXiv preprint arXiv:2305.18565*, 2023. 1
- [7] Yuxin Chen, Yiran Zhao, Yang Zhang, An Zhang, Kenji Kawaguchi, Shafiq Joty, Junnan Li, Tat-Seng Chua, Michael Qizhe Shieh, and Wenxuan Zhang. The emergence of abstract thought in large language models beyond any language. *arXiv preprint arXiv:2506.09890*, 2025. 1, 3, 11
- [8] Zhe Chen, Jiannan Wu, Wenhai Wang, Weijie Su, Guo Chen, Sen Xing, Muyan Zhong, Qinglong Zhang, Xizhou Zhu, Lewei Lu, et al. Internvl: Scaling up vision foundation models and aligning for generic visual-linguistic tasks. In *Proceedings of the IEEE/CVF Conference on Computer Vision and Pattern Recognition*, pages 24185–24198, 2024. 1, 4, 7
- [9] Karl Cobbe, Vineet Kosaraju, Mohammad Bavarian, Mark Chen, Heewoo Jun, Lukasz Kaiser, Matthias Plappert, Jerry Tworek, Jacob Hilton, Reiichiro Nakano, Christopher Hesse, and John Schulman. Training verifiers to solve math word problems. *arXiv preprint arXiv:2110.14168*, 2021. 3
- [10] Damai Dai, Li Dong, Yaru Hao, Zhifang Sui, Baobao Chang, and Furu Wei. Knowledge neurons in pretrained transformers. *arXiv preprint arXiv:2104.08696*, 2021. 3
- [11] Rocktim Jyoti Das, Simeon Emilov Hristov, Haonan Li, Dimitar Iliyanov Dimitrov, Ivan Koychev, and Preslav Nakov. Exams-v: A multi-discipline multilingual multimodal exam benchmark for evaluating vision language models. *arXiv preprint arXiv:2403.10378*, 2024. 2
- [12] Yue Fan, Xuehai He, Diji Yang, Kaizhi Zheng, Ching-Chen Kuo, Yuting Zheng, Sravana Jyothi Narayanaraju, Xinze Guan, and Xin Eric Wang. Grit: Teaching mllms to think with images, 2025. 7
- [13] Kaituo Feng, Kaixiong Gong, Bohao Li, Zonghao Guo, Yibing Wang, Tianshuo Peng, Benyou Wang, and Xiangyu Yue. Video-rl: Reinforcing video reasoning in mllms. <https://huggingface.co/Video-R1/Qwen2.5-VL-7B-COT-SFT>, 2025. Paper introducing Video-R1 datasets, models, and training pipeline. 7
- [14] Jonathan Frankle and Michael Carbin. The lottery ticket hypothesis: Finding sparse, trainable neural networks. *arXiv preprint arXiv:1803.03635*, 2018. 3
- [15] Chaoyou Fu, Peixian Chen, Yunhang Shen, Yulei Qin, Mengdan Zhang, Xu Lin, Jinrui Yang, Xiawu Zheng, Ke Li, Xing Sun, Yunsheng Wu, and Rongrong Ji. Mme: A comprehensive evaluation benchmark for multimodal large language models, 2024. 7, 16
- [16] Mor Geva, Roei Schuster, Jonathan Berant, and Omer Levy. Transformer feed-forward layers are key-value memories. *arXiv preprint arXiv:2012.14913*, 2020. 3
- [17] Daya Guo, Dejian Yang, Haowei Zhang, Junxiao Song, Ruoyu Zhang, Runxin Xu, Qihao Zhu, Shirong Ma, Peiyi Wang, Xiao Bi, et al. Deepseek-r1: Incentivizing reasoning capability in llms via reinforcement learning. *arXiv preprint arXiv:2501.12948*, 2025. 1, 4, 7

- [18] Yunzhuo Hao, Jiawei Gu, Huichen Will Wang, Linjie Li, Zhengyuan Yang, Lijuan Wang, and Yu Cheng. Can mllms reason in multimodality? emma: An enhanced multimodal reasoning benchmark. *arXiv preprint arXiv:2501.05444*, 2025. 1
- [19] Andrej Karpathy, Justin Johnson, and Li Fei-Fei. Visualizing and understanding recurrent networks. *arXiv preprint arXiv:1506.02078*, 2015. 3
- [20] Hugo Laurençon, Andrés Marafioti, Victor Sanh, and Léo Tronchon. Building and better understanding vision-language models: insights and future directions. *arXiv preprint arXiv:2408.12637*, 2024. 1, 7
- [21] Jixuan Leng, Chengsong Huang, Langlin Huang, Bill Yuchen Lin, William W Cohen, Haohan Wang, and Jiaxin Huang. Crosswordbench: Evaluating the reasoning capabilities of llms and lvlms with controllable puzzle generation. *arXiv preprint arXiv:2504.00043*, 2025. 1
- [22] Bo Li, Yuanhan Zhang, Dong Guo, Renrui Zhang, Feng Li, Hao Zhang, Kaichen Zhang, Peiyuan Zhang, Yanwei Li, Ziwei Liu, et al. Llava-onevision: Easy visual task transfer. *arXiv preprint arXiv:2408.03326*, 2024. 2
- [23] Junnan Li, Dongxu Li, Silvio Savarese, and Steven Hoi. Blip-2: Bootstrapping language-image pre-training with frozen image encoders and large language models. In *International conference on machine learning*, pages 19730–19742. PMLR, 2023. 1
- [24] Yifan Li, Yifan Du, Kun Zhou, Jinpeng Wang, Wayne Xin Zhao, and Ji-Rong Wen. Evaluating object hallucination in large vision-language models. *arXiv preprint arXiv:2305.10355*, 2023. 7, 16
- [25] Haotian Liu, Chunyuan Li, Qingyang Wu, and Yong Jae Lee. Visual instruction tuning. *Advances in neural information processing systems*, 36:34892–34916, 2023. 2
- [26] Haotian Liu, Chunyuan Li, Yuheng Li, Bo Li, Yuanhan Zhang, Sheng Shen, and Yong Jae Lee. Llava-next: Improved reasoning, ocr, and world knowledge, 2024. 4, 7
- [27] Xiaohao Liu, Jie Wu, Zhulin Tao, Yunshan Ma, Yinwei Wei, and Tat-seng Chua. Fine-tuning multimodal large language models for product bundling. In *Proceedings of the 31st ACM SIGKDD Conference on Knowledge Discovery and Data Mining V. 1*, pages 848–858, 2025. 1
- [28] Zijun Liu, Peiyi Wang, Runxin Xu, Shirong Ma, Chong Ruan, Peng Li, Yang Liu, and Yu Wu. Inference-time scaling for generalist reward modeling. *arXiv preprint arXiv:2504.02495*, 2025. 2
- [29] Pan Lu, Ran Gong, Shibiao Jiang, Liang Qiu, Siyuan Huang, Xiaodan Liang, and Song-Chun Zhu. Inter-gps: Interpretable geometry problem solving with formal language and symbolic reasoning. *arXiv preprint arXiv:2105.04165*, 2021. 3
- [30] Pan Lu, Hritik Bansal, Tony Xia, Jiacheng Liu, Chunyuan Li, Hannaneh Hajishirzi, Hao Cheng, Kai-Wei Chang, Michel Galley, and Jianfeng Gao. Mathvista: Evaluating mathematical reasoning of foundation models in visual contexts. *arXiv preprint arXiv:2310.02255*, 2023. 4, 7, 16
- [31] Jesse Mu and Jacob Andreas. Compositional explanations of neurons. *Advances in Neural Information Processing Systems*, 33:17153–17163, 2020. 3
- [32] OpenAI. Multimodal neurons in artificial neural networks. <https://openai.com/index/multimodal-neurons/>, 2021. Accessed: 2025-09-07. 3
- [33] OpenAI. Language models can explain neurons in language models. <https://openai.com/index/language-models-can-explain-neurons-in-language-models/>, 2023. Accessed: 2025-09-07. 3
- [34] Zhiliang Peng, Wenhui Wang, Li Dong, Yaru Hao, Shaohan Huang, Shuming Ma, and Furu Wei. Kosmos-2: Grounding multimodal large language models to the world. *arXiv preprint arXiv:2306.14824*, 2023. 1
- [35] Kangan Qian, Sicong Jiang, Yang Zhong, Ziang Luo, Zilin Huang, Tianze Zhu, Kun Jiang, Mengmeng Yang, Zheng Fu, Jinyu Miao, et al. Agentthink: A unified framework for tool-augmented chain-of-thought reasoning in vision-language models for autonomous driving. *arXiv preprint arXiv:2505.15298*, 2025. 2
- [36] Alec Radford, Rafal Jozefowicz, and Ilya Sutskever. Learning to generate reviews and discovering sentiment. 2018. 2
- [37] Alec Radford, Jong Wook Kim, Chris Hallacy, Aditya Ramesh, Gabriel Goh, Sandhini Agarwal, Girish Sastry, Amanda Askell, Pamela Mishkin, Jack Clark, et al. Learning transferable visual models from natural language supervision. In *International conference on machine learning*, pages 8748–8763. PmLR, 2021. 2
- [38] Tanik Saikh, Tirthankar Ghosal, Amish Mittal, Asif Ekbal, and Pushpak Bhattacharyya. Scienceqa: A novel resource for question answering on scholarly articles. *International Journal on Digital Libraries*, 23(3):289–301, 2022. 7, 16
- [39] Yugen Sato and Tomohiro Takagi. Identifying multi-modal knowledge neurons in pretrained transformers via two-stage filtering. *arXiv preprint arXiv:2503.22941*, 2025. 3
- [40] Hao Shao, Shengju Qian, Han Xiao, Guanglu Song, Zhuofan Zong, Letian Wang, Yu Liu, and Hongsheng Li. Visual cot: Advancing multi-modal language models with a comprehensive dataset and benchmark for chain-of-thought reasoning. *Advances in Neural Information Processing Systems*, 37:8612–8642, 2024. 2
- [41] Haozhan Shen, Peng Liu, Jingcheng Li, Chunxin Fang, Yibo Ma, Jiajia Liao, Qiaoli Shen, Zilun Zhang, Kangjia Zhao, Qianqian Zhang, et al. Vlm-r1: A stable and generalizable r1-style large vision-language model. *arXiv preprint arXiv:2504.07615*, 2025. 7
- [42] Kimi Team, Angang Du, Bohong Yin, Bowei Xing, Bowen Qu, Bowen Wang, Cheng Chen, Chenlin Zhang, Chenzhuang Du, Chu Wei, et al. Kimi-vl technical report. *arXiv preprint arXiv:2504.07491*, 2025. 2
- [43] Curt Tigges, Michael Hanna, Qinan Yu, and Stella Biderman. Llm circuit analyses are consistent across training and scale. *Advances in Neural Information Processing Systems*, 37:40699–40731, 2024. 1
- [44] Leandro von Werra, Younes Belkada, Lewis Tunstall, Edward Beeching, Tristan Thrush, Nathan Lambert, Shengyi Huang, Kashif Rasul, and Quentin Gallouédec. TRL: Transformer Reinforcement Learning. <https://huggingface.co/shawnzzzzz/Qwen2.5-VL-7B-Open-R1-Distill>, 2020. 7

- [45] Weiyun Wang, Zhe Chen, Wenhai Wang, Yue Cao, Yangzhou Liu, Zhangwei Gao, Jinguo Zhu, Xizhou Zhu, Lewei Lu, Yu Qiao, and Jifeng Dai. Enhancing the reasoning ability of multimodal large language models via mixed preference optimization. *arXiv preprint arXiv:2411.10442*, 2024. 2
- [46] Xiaozhi Wang, Kaiyue Wen, Zhengyan Zhang, Lei Hou, Zhiyuan Liu, and Juanzi Li. Finding skill neurons in pre-trained transformer-based language models. *arXiv preprint arXiv:2211.07349*, 2022. 3
- [47] Xiaokun Wang, Peiyu Wang, Jiangbo Pei, Wei Shen, Yi Peng, Yunzhuo Hao, Weijie Qiu, Ai Jian, Tianyidan Xie, Xuchen Song, et al. Skywork-v1 reward: An effective reward model for multimodal understanding and reasoning. *arXiv preprint arXiv:2505.07263*, 2025. 2
- [48] Hongchen Wei and Zhenzhong Chen. Training-free reasoning and reflection in mllms. *arXiv preprint arXiv:2505.16151*, 2025. 7
- [49] Williammsq. Qwen2.5-3b-instruct-math-grpo. <https://huggingface.co/Williammsq/Qwen2.5-3B-Instruct-Math-GRPO>, 2025. Accessed: 2025-09-08. 4, 7
- [50] Mitchell Wortsman, Gabriel Ilharco, Samir Ya Gadre, Rebecca Roelofs, Raphael Gontijo-Lopes, Ari S Morcos, Hongseok Namkoong, Ali Farhadi, Yair Carmon, Simon Kornblith, et al. Model soups: averaging weights of multiple fine-tuned models improves accuracy without increasing inference time. In *International conference on machine learning*, pages 23965–23998. PMLR, 2022. 7
- [51] John M Wu, Yonatan Belinkov, Hassan Sajjad, Nadir Durani, Fahim Dalvi, and James Glass. Similarity analysis of contextual word representation models. *arXiv preprint arXiv:2005.01172*, 2020. 1
- [52] An Yang, Beichen Zhang, Binyuan Hui, Bofei Gao, Bowen Yu, Chengpeng Li, Dayiheng Liu, Jianhong Tu, Jingren Zhou, Junyang Lin, et al. Qwen2.5-math technical report: Toward mathematical expert model via self-improvement. *arXiv preprint arXiv:2409.12122*, 2024. 1, 4, 7
- [53] Le Yu, Bowen Yu, Haiyang Yu, Fei Huang, and Yongbin Li. Language models are super mario: Absorbing abilities from homologous models as a free lunch. In *Forty-first International Conference on Machine Learning*, 2024. 7
- [54] Xiang Yue, Yuansheng Ni, Kai Zhang, Tianyu Zheng, Ruoqi Liu, Ge Zhang, Samuel Stevens, Dongfu Jiang, Weiming Ren, Yuxuan Sun, et al. Mmmu: A massive multi-discipline multimodal understanding and reasoning benchmark for expert agi. In *Proceedings of the IEEE/CVF Conference on Computer Vision and Pattern Recognition*, pages 9556–9567, 2024. 7, 16
- [55] Xiang Yue, Tianyu Zheng, Yuansheng Ni, Yubo Wang, Kai Zhang, Shengbang Tong, Yuxuan Sun, Botao Yu, Ge Zhang, Huan Sun, et al. Mmmu-pro: A more robust multi-discipline multimodal understanding benchmark. *arXiv preprint arXiv:2409.02813*, 2024. 7, 16
- [56] Xiang Yue, Tianyu Zheng, Yuansheng Ni, Yubo Wang, Kai Zhang, Shengbang Tong, Yuxuan Sun, Botao Yu, Ge Zhang, Huan Sun, et al. Mmmu-pro: A more robust multi-discipline multimodal understanding benchmark. *arXiv preprint arXiv:2409.02813*, 2024. 1, 2
- [57] Ruohong Zhang, Bowen Zhang, Yanghao Li, Haotian Zhang, Zhiqing Sun, Zhe Gan, Yinfei Yang, Ruoming Pang, and Yiming Yang. Improve vision language model chain-of-thought reasoning. *arXiv preprint arXiv:2410.16198*, 2024. 1
- [58] Yuhao Zhang, Hang Jiang, Yasuhide Miura, Christopher D Manning, and Curtis P Langlotz. Contrastive learning of medical visual representations from paired images and text. In *Machine learning for healthcare conference*, pages 2–25. PMLR, 2022. 2
- [59] Zhuosheng Zhang, Aston Zhang, Mu Li, Hai Zhao, George Karypis, and Alex Smola. Multimodal chain-of-thought reasoning in language models. *arXiv preprint arXiv:2302.00923*, 2023. 2
- [60] Deyao Zhu, Jun Chen, Xiaoqian Shen, Xiang Li, and Mohamed Elhoseiny. Minigt-4: Enhancing vision-language understanding with advanced large language models. *arXiv preprint arXiv:2304.10592*, 2023. 2
- [61] Brianna Zitkovich, Tianhe Yu, Sichun Xu, Peng Xu, Ted Xiao, Fei Xia, Jialin Wu, Paul Wohlhart, Stefan Welker, Ayzaan Wahid, et al. Rt-2: Vision-language-action models transfer web knowledge to robotic control. In *Conference on Robot Learning*, pages 2165–2183. PMLR, 2023. 1

A. Neuron Detection Algorithm

Inspired by prior work [5, 7], we adopt a *parallelizable neuron detection method*. Unlike the main definition in Eq. (4), which considers the change in the *final* output embedding after deactivating a neuron, here we compute the impact *locally at the layer containing the neuron*. This layer-wise impact serves as a proxy (or component) for the overall impact while being far more efficient to compute.

Formally, let $X \in \mathbb{R}^{l \times d_{\text{model}}}$ denote the hidden states input to a given layer, where l is the sequence length and d_{model} the hidden dimension. For a neuron N in this layer, its impact is measured as:

$$\|f(X; \theta) - f(X; \theta^{\uparrow N})\|_2, \quad (14)$$

where $f(X; \theta)$ is the layer output with parameters θ , and $f(X; \theta^{\uparrow N})$ is the output when neuron N is deactivated (i.e., its parameters are set to zero).

A.1. Feed-Forward Neurons

A standard feed-forward network (FFN) layer can be written as:

$$\text{FFN}(X) = (\text{SiLU}(XW_{\text{gate}}) \odot (XW_{\text{up}}))W_{\text{down}}, \quad (15)$$

where $W_{\text{gate}}, W_{\text{up}} \in \mathbb{R}^{d_{\text{model}} \times d_{\text{inter}}}$ and $W_{\text{down}} \in \mathbb{R}^{d_{\text{inter}} \times d_{\text{model}}}$. The intermediate activation is:

$$H_{\text{act}} = \text{SiLU}(XW_{\text{gate}}) \odot (XW_{\text{up}}) \in \mathbb{R}^{l \times d_{\text{inter}}}. \quad (16)$$

Deactivating the k -th intermediate neuron corresponds to zeroing out the k -th column $H_{\text{act}}[:, k]$, which is equivalent to removing the k -th feature before multiplication with W_{down} . The resulting change in output is:

$$\Delta Y_{\text{FFN},k} = H_{\text{act}}[:, k] \cdot (W_{\text{down}})_{k,:}. \quad (17)$$

Thus, the impact of neuron k is the squared L2 norm:

$$\|\Delta Y_{\text{FFN},k}\|^2 = \|H_{\text{act}}[:, k](W_{\text{down}})_{k,:}\|^2. \quad (8)$$

This can be computed in parallel for all $k \in \{1, \dots, d_{\text{inter}}\}$.

A.2. Self-Attention Neurons

For a single-head self-attention layer:

$$Y_{\text{Attn}} = \text{Softmax}\left(\frac{QK^\top}{\sqrt{d_k}}\right) V, \quad (18)$$

with $Q = XW_Q$, $K = XW_K$, $V = XW_V$. The attention matrix is $A = \text{Softmax}(QK^\top/\sqrt{d_k})$, yielding output $Y_{\text{Attn}} = AV$.

(a) Value Neurons (W_V)

A neuron defined by column k of W_V sets $V[:, k]$ to zero when deactivated. The change in output is:

$$\Delta Y_{\text{Attn},k}^{(V)} = AV[:, k], \quad (19)$$

and the impact is:

$$\|\Delta Y_{\text{Attn},k}^{(V)}\|^2 = \|AV[:, k]\|^2. \quad (10)$$

(b) Query Neurons (W_Q)

Deactivating the k -th column of W_Q zeroes $Q[:, k]$, which alters the unnormalized attention scores:

$$\Delta S_{\text{raw},k} = \frac{Q[:, k](K[:, k])^\top}{\sqrt{d_k}}. \quad (20)$$

This modifies the attention matrix from $A_{\text{orig}} = \text{softmax}(S_{\text{raw}})$ to $A^{\uparrow N_{Q,k}} = \text{softmax}(S_{\text{raw}} - \Delta S_{\text{raw},k})$. The resulting change in output is:

$$\Delta Y_{\text{Attn},k}^{(Q)} = (A_{\text{orig}} - A^{\uparrow N_{Q,k}})V, \quad (21)$$

and its impact is:

$$\|\Delta Y_{\text{Attn},k}^{(Q)}\|^2. \quad (11)$$

(c) Key Neurons (W_K)

The effect of deactivating a key neuron is *symmetric* to that of query neurons, since the change term

$$\Delta S_{\text{raw},k} = \frac{Q[:, k](K[:, k])^\top}{\sqrt{d_k}} \quad (22)$$

captures the interaction between query and key neurons along dimension k . Thus, query and key neurons are dual roles in shaping the attention scores.

A.3. Equivalence of Query and Value Impacts

Although the mechanics differ—query/key neurons alter the *attention weights*, while value neurons alter the *content propagated*—their impact is functionally equivalent in our parallel detection framework:

- Both are measured as L2 changes in the attention output Y_{Attn} .
- A query neuron modifies the distribution A over tokens, indirectly scaling the contribution of values.
- A value neuron directly zeroes out one content column, effectively applying a structured mask on V .

Therefore, in practice, `attn.q` and `attn.v` neurons are comparable impact carriers, differing only in whether they modulate weights (Q) or content (V).

B. Theory and Proofs for Section 5.3

Setup. We compare SNRF (Eq. 11) with linear merging:

$$\begin{aligned} \widetilde{W}^{\text{lin}} &= W^{\text{tgt}} + \beta \Delta, \\ \Delta &= W^{\text{src}} - W^{\text{tgt}}. \end{aligned} \quad (23)$$

For theory, we suppress (ℓ, p) and work with a single block W . Let S denote the shared-inference coordinates (Sec. 5), with projectors P_S and P_\perp . We decompose the update as

$$\Delta_S := P_S \Delta, \quad \Delta_\perp := P_\perp \Delta.$$

SNRF applies a masked rank- r update inside S :

$$\begin{aligned} \widetilde{W}^{\text{snrf}} &= W^{\text{tgt}} + \beta P_S(\Delta^{(r)}), \\ \Delta^{\text{snrf}} &= \Delta_S^{(r)}, \\ \Delta^{\text{lin}} &= \Delta_S + \Delta_\perp, \end{aligned} \quad (24)$$

where $\Delta_S^{(r)}$ is the rank- r truncated SVD of Δ_S .

Main result. For sufficiently small β ,

$$\begin{aligned} \Delta \mathcal{L}_{\text{lin}}(\beta) - \Delta \mathcal{L}_{\text{snrf}}(\beta) &\geq \underbrace{\frac{\beta^2}{2} \mu_\perp \|\Delta_\perp\|_F^2}_{\text{curvature in } S^\perp \text{ (lin only)}} \\ &\quad - \underbrace{\frac{\beta^2}{2} \mu_S \|\Delta_S - \Delta_S^{(r)}\|_F^2}_{\text{low-rank truncation (SNRF only)}} \\ &\quad - \underbrace{\beta c \|P_S g\|_F \|\Delta\|_F}_{\text{leakage}} + O(\beta^3), \end{aligned} \quad (25)$$

where $c = \varepsilon(1 + \eta)$ is small.

Whenever

$$\mu_\perp \|\Delta_\perp\|_F^2 > \mu_S \|\Delta_S - \Delta_S^{(r)}\|_F^2 + c \beta^{-1} \|P_S g\|_F \|\Delta\|_F, \quad (26)$$

we obtain $\Delta\mathcal{L}_{\text{snrf}}(\beta) < \Delta\mathcal{L}_{\text{lin}}(\beta)$.

Thus, for sufficiently small β , linear merging incurs a strictly higher loss due to movement in S^\perp , where curvature is large. SNRF masks S^\perp and pays only the in- S truncation error—which vanishes whenever $r = \text{rank}(\Delta_S)$ and is minimized otherwise by the truncated SVD.

Assumptions (A1-A4).

- (i) Gradient concentrates in S : $\|P_\perp g\|_F \leq \varepsilon \|P_S g\|_F$.
- (ii) Curvature gap: $H \succeq \mu_S P_S + \mu_\perp P_\perp$ with $0 < \mu_S \leq \mu_\perp$.
- (iii) First-order signal aligns with S : $\langle P_\perp g, \Delta_\perp \rangle \geq -\eta \|P_\perp g\|_F \|\Delta_\perp\|_F$.
- (iv) $\Delta_S^{(r)}$ is the best rank- r approximation of Δ_S (Eckart-Young-Mirsky).

Taylor expansions. At W^{tgt} , let $g = \nabla\mathcal{L}(W)$ and $H = \nabla^2\mathcal{L}(W)$:

$$\Delta\mathcal{L}_{\text{lin}}(\beta) = \beta \langle g, \Delta \rangle + \frac{\beta^2}{2} \langle \Delta, H\Delta \rangle + O(\beta^3), \quad (27)$$

$$\Delta\mathcal{L}_{\text{snrf}}(\beta) = \beta \langle g, \Delta_S^{(r)} \rangle + \frac{\beta^2}{2} \langle \Delta_S^{(r)}, H\Delta_S^{(r)} \rangle + O(\beta^3). \quad (28)$$

Quadratic terms via curvature gap. Decompose $\Delta = \Delta_S + \Delta_\perp$. Using $H \succeq \mu_S P_S + \mu_\perp P_\perp$,

$$\langle \Delta, H\Delta \rangle \geq \mu_S \|\Delta_S\|_F^2 + \mu_\perp \|\Delta_\perp\|_F^2, \quad \langle \Delta_S^{(r)}, H\Delta_S^{(r)} \rangle \geq \mu_S \|\Delta_S^{(r)}\|_F^2.$$

Hence,

$$\langle \Delta, H\Delta \rangle - \langle \Delta_S^{(r)}, H\Delta_S^{(r)} \rangle \geq \mu_\perp \|\Delta_\perp\|_F^2 - \mu_S \|\Delta_S - \Delta_S^{(r)}\|_F^2.$$

First-order difference and leakage.

$$\langle g, \Delta \rangle - \langle g, \Delta_S^{(r)} \rangle = \langle P_S g, \Delta_S - \Delta_S^{(r)} \rangle + \langle P_\perp g, \Delta_\perp \rangle.$$

By Cauchy-Schwarz and (A1)-(A3):

$$\langle P_S g, \Delta_S - \Delta_S^{(r)} \rangle \leq \|P_S g\|_F \|\Delta_S - \Delta_S^{(r)}\|_F,$$

$$\langle P_\perp g, \Delta_\perp \rangle \geq -\eta \|P_\perp g\|_F \|\Delta_\perp\|_F \geq -\eta\varepsilon \|P_S g\|_F \|\Delta\|_F.$$

Low-rank optimality in S . By Eckart-Young-Mirsky, $\Delta_S^{(r)}$ minimizes $\|\Delta_S - \hat{\Delta}\|_F$ over all rank- r matrices $\hat{\Delta}$.

Collecting terms. Combining the bounds above with the Taylor expansion yields Eq. 25. Condition 26 ensures that the positive quadratic advantage from masking S^\perp dominates both truncation and leakage terms, establishing $\Delta\mathcal{L}_{\text{snrf}}(\beta) < \Delta\mathcal{L}_{\text{lin}}(\beta)$ for sufficiently small β . \square

C. Experimental details for Findings OF Shared Neurons Basis

C.1. Finding 1

Strong Overlap. Across the five representative model pairs shown in Figure 8, we consistently observe substantial overlap in inference-related neurons: Qwen2.5-VL-7B vs. Qwen2.5-Math-7B share 4,703 neurons (74.5% of the union) with only 667 (10.6%) and 942 (14.9%) remaining model-specific; Intern2.5-VL-4B vs. Qwen2.5-GRPO-3B share 2,967 (71.3%); Idefics3-8B vs. Deepseek-LLaMA3-8B share 5,069 (71.5%); Qwen2.5-VL-3B vs. Qwen2.5-GRPO-3B share 2,645 (68.3%); and even the cross-backbone pair LLaVA-Next-8B vs. Deepseek-LLaMA3-8B retains 5,146 (48.0%) shared neurons. Layer-module inspection (Figure 9 and 10) shows that these shared neurons concentrate in `attn.k` with secondary presence in `attn.v`, forming two prominent clusters in early layers (before layer 6) and late layers (after layer 20), consistent with roles in generic semantic parsing and high-level inference. Notably, strong overlaps also occur between models without identical language backbones, pointing to universal inference units that transcend architecture and training objectives. Causal ablation confirms their functional importance: zeroing parameters exclusively associated with the shared set ($\mathcal{N}_{\text{shared}}$) leads to a much larger drop in inference accuracy than randomly ablating an equal number of neurons, demonstrating that these shared neurons form a core inference substrate reused across modalities and model families. Additionally, as shown in Figure 8, we observe that even models of different types share a substantial number of neurons.

Where the shared neurons live. Building on the main-text observations for Qwen2.5-VL-7B and Qwen2.5-Math-7B, we further examine how shared neurons distribute across layers and modules in other model pairs. As shown in Figure 4, the shared neurons in **Intern2.5-VL-4B** and **Qwen2.5-GRPO-3B** are predominantly concentrated in the `attn.k` matrices across almost all layers, with a consistent but smaller secondary presence in `attn.v`. Only a handful of early layers (e.g., layers 1–3) and a few middle or late layers display modest activity in the `fwd_down` or `fwd_up` modules. Notably, Intern2.5-VL-4B exhibits an additional rise in shared-neuron counts in the upper layers (around layer 30 and beyond), indicating a stronger reliance on key-vector sharing during deep decoding, whereas Qwen2.5-GRPO-3B shows relatively more `attn.v` sharing in the earliest layers, suggesting richer value-vector interactions during initial feature capture.

A similar pattern appears for **Idefics3-LLaMA-8B** and **Deepseek-LLaMA3-8B**. Here, `attn.k` again dominates the shared-neuron distribution and `attn.v` provides a sec-

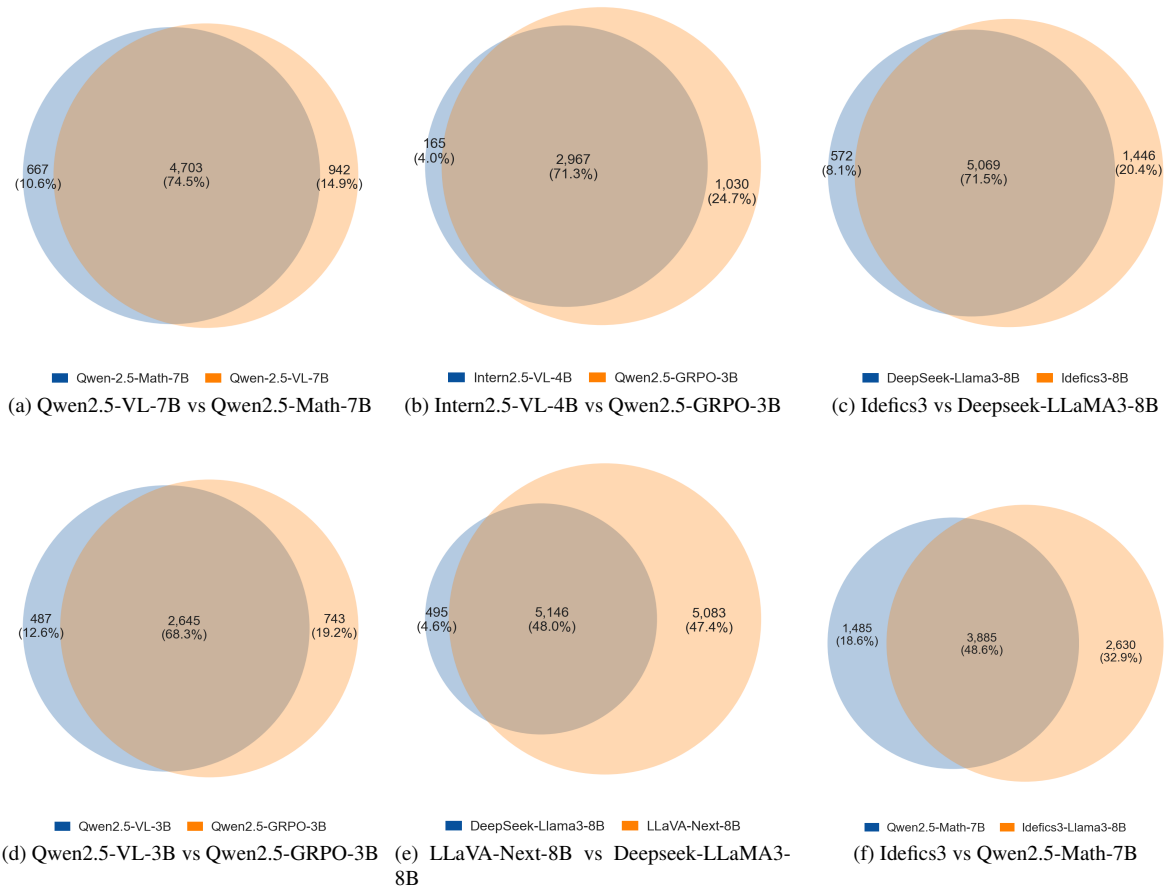


Figure 8. Overlap of activated neurons across different LVM families.

ondary contribution, while `fwd_down` and `fwd_up` remain consistently minor with only localized peaks in the very first or final layers. Unlike the Qwen family, however, these two models show a relatively flat, plateau-like distribution through the middle layers (approximately layers 5–15) and a sharp spike in the very first one or two layers, pointing to a particularly heavy demand for shared neurons during the initial embedding-fusion stage.

Overall, despite architectural differences, all examined models exhibit a global regularity: shared neurons overwhelmingly reside in `attn.k`, with `attn.v` consistently secondary. This pattern underscores the central role of attention key vectors in cross-model knowledge sharing and transfer.

C.2. Fing 2

More experiments on deactivation experiments. We evaluate the *causal* role of shared neurons ($\mathcal{N}_{\text{shared}}$; Eq. 6) by (i) **Deact**—zeroing the parameters that produce/consume only neurons in $\mathcal{N}_{\text{shared}}$; and (ii) **Random Deact**—ablating the *same number* of neurons sampled at random from the

same layer-module budget.

Table 3 summarizes the results across MATHVISTA (CoT/Format/Solution), MME, POPE, ScienceQA, MMMU and MMMU-Pro (V). Across three LVMs, deactivating the shared neurons collapses performance to **0.0** on every metric, whereas random ablations of equal size lead to a moderate drop only. This pattern holds consistently, demonstrating that $\mathcal{N}_{\text{shared}}$ are both *necessary* and *specific* for multi-step inference.

C.3. Fing 3

More Cases. Using our amplification intervention, from Figure 11 presents six cases. In Idefics3’s feed-forward down-projection, `ide.fwd.down.L21.N516` (a) favors subword fragments composed of letters and symbols (mixed case letters, hyphens, Greek marks), indicating sensitivity to morphological pieces; `ide.fwd.down.L7.N8196` (b) instead concentrates on brackets, digits, and simple operators, reflecting selectivity for equation layout. In LLaMA3, the attention value channel `LLaMA3.attn.v.L3.N2052` (c)

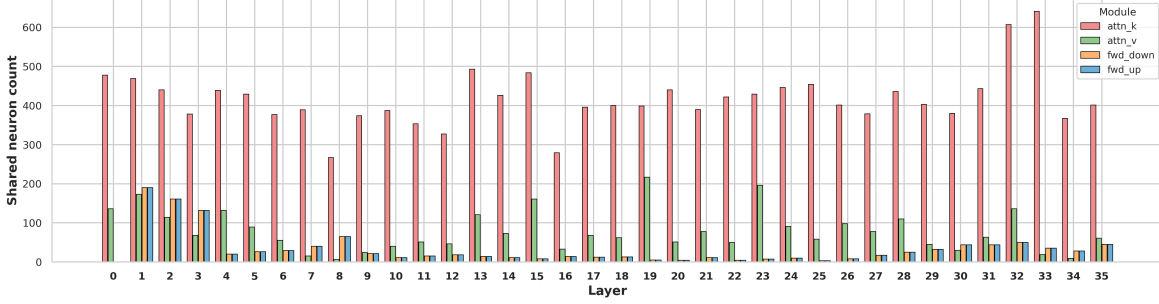


Figure 9. Distribution of shared neurons across layers and modules in Intern2.5-VL-4B and Qwen2.5-GRPO-3B.

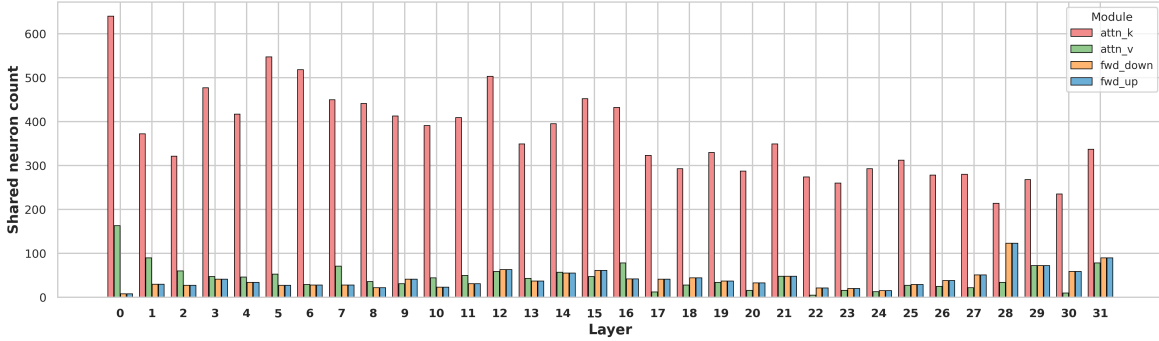


Figure 10. Distribution of shared neurons across layers and modules in Idefics3-LLaMA-8B and Deepseek-LLaMA3-8B.

repeatedly activates on high-frequency function words and number words (e.g., “the,” ordinals/cardinals), suggesting a role in anchoring syntax and count-related context, while the feed-forward down-projection LLaMA3.fwd.down.L0.N2378 (d) responds more to sentence boundaries and punctuation (right parentheses, periods), encoding formatting cues. Across models, Intern2.5-VL’s intern.fwd.down.L0.N2378 (e) shows a strong bias toward numerals and operators, whereas Qwen-3B’s qwen3b.attn.v.L0.N2378 (f) highlights topical clusters (e.g., cryptography, the “re-” prefix). Altogether, these word clouds indicate that, even across models and layers, individual neurons consistently carry sub-domain semantics—digits/operators, typography/punctuation, syntactic anchors, and topical terms—supporting their utility as actionable semantic carriers for structured interpretability and targeted control.

Statistical Analysis We conducted a statistical analysis of the math-related associations within the neurons’ top-10 amplified tokens. Using GPT-4o as a classification model, we categorized each token to determine whether it is associated with mathematical concepts. Let \mathcal{N} denote the set of neurons, and for each neuron $i \in \mathcal{N}$, let $T_i = \{t_{i1}, t_{i2}, \dots, t_{iK}\}$ represent the top- K amplified tokens, with $K = 10$ in our analysis. Define the indicator

function:

$$\mathbf{1}_{\text{math}}(t) = \begin{cases} 1, & \text{if token } t \text{ is classified as math-related,} \\ 0, & \text{otherwise.} \end{cases}$$

As shown in Figure 12, the math neuron ratios differ across text and vision models. Text models (blue) generally contain a higher proportion of math-related neurons, with Qwen2.5-Math-7B reaching 96.3% and LLaMA3 at 76.4%. Vision-language models (red) also exhibit strong math sensitivity, for example Qwen2.5-VL-7B at 80.4% and Idefics-LLaMA3 at 78.8%. These results indicate that both text and vision models encode substantial mathematical knowledge, and that inference capabilities are closely tied to neurons sensitive to mathematical tokens.

These results show that a significant proportion of shared neurons encode mathematical knowledge.

D. Details about experiments

D.1. Exact model specs and checkpoints

Below are the vision-language models we evaluate, along with their parameter scales, language backbones, paired text models (for parameter-merging where applicable), and official checkpoints.

All models use their authors’ officially released vision encoders. For parameter merging, we follow the published

Model	MathVista-Cot	Format	Solution	MME	POPE	SCIQA	MMMU	MMMU-Pro (V)
<i>Base</i>								
QwenVL-7B	48.8	68.8	37.5	1681	86.2	54.5	0.503	0.116
QwenVL-3B	52.6	61.6	50.8	1535	87.2	52.5	0.461	0.018
Intern2.5-VL-4B	60.4	65.1	61.6	1670	90.8	97.4	0.491	0.000
<i>Deact (shared)</i>								
QwenVL-7B	0.0	0.0	0.0	0	0.0	0.0	0.000	0.000
QwenVL-3B	0.0	0.0	0.0	0	0.0	0.0	0.000	0.000
Intern2.5-VL-4B	0.0	0.0	0.0	0	0.0	0.0	0.000	0.000
<i>Random Deact</i>								
QwenVL-7B	36.4	47.2	32.6	1510	75.9	45.6	0.482	0.081
QwenVL-3B	32.6	32.1	32.1	1242	74.5	34.1	0.393	0.004
Intern2.5-VL-4B	34.4	34.3	36.2	1353	82.2	63.4	0.272	0.000

Table 3. **Effect of ablating shared neurons across benchmarks.** Removing $\mathcal{N}_{\text{shared}}$ collapses performance to zero, while random ablations of the same size only moderately reduce scores. Higher is better for all metrics.

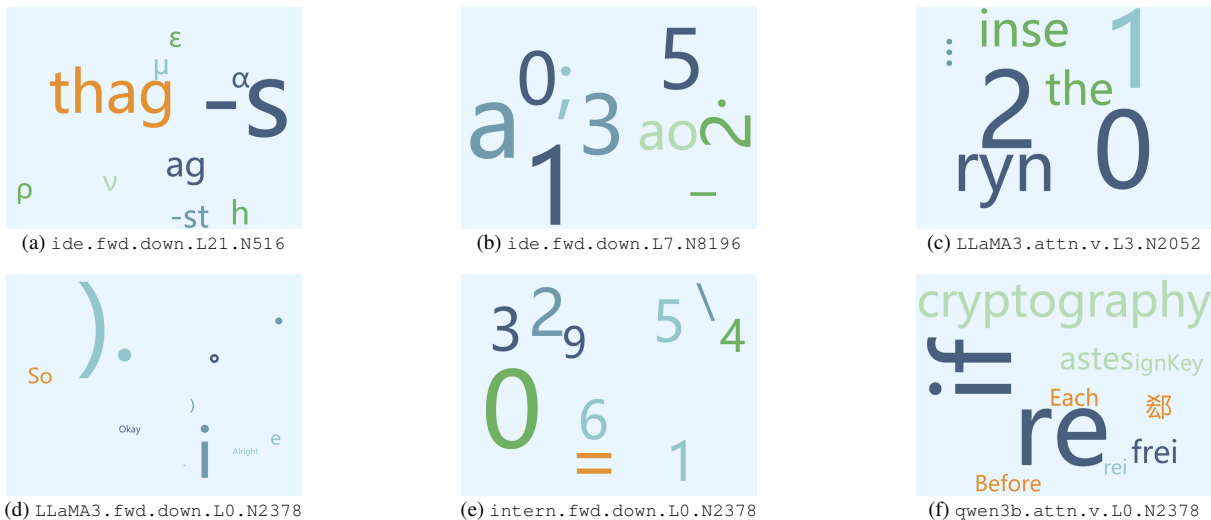


Figure 11. Word clouds of token concepts for different neurons.

pairing: e.g. Qwen2.5-VL-7B is paired with the Qwen2.5-Math text model; Intern2.5-VL-4B is paired with Qwen3B-GRPO (or equivalent text model) in our merging setup. Model licenses are as released on their model hub pages (e.g. Apache-2.0 for most).

D.2. Details about benchmarks

We conduct experiments on six representative multimodal benchmarks—MathVista [30], *MME* [15], *POPE* [24], *ScienceQA* [38], *MMMU* [54], and *MMMU-Pro* [55]. These benchmarks jointly span visual mathematical inference (MathVista), broad perception and cognition (MME), hallucination detection (POPE), multimodal science question answering with explanations (ScienceQA), and college-level multi-discipline understanding and inference (MMMU and MMMU-Pro). Together they allow us to measure modality alignment, perception→inference competence, and safety/-

calibration under diverse conditions.

MathVista provides over six thousand high-quality visual math problems covering functions, geometry, algebra, and real-world quantitative inference. We follow the official split by using the small *testmini* set for ablations and reporting final results on the hidden *test* set via the evaluation server. MME evaluates a wide spectrum of perception and inference sub-tasks such as fine-grained recognition, text understanding, logical inference, and commonsense; it provides only a test-style question-answer collection without train/validation subsets and is therefore used in a strict zero/low-shot setting. POPE is designed for hallucination detection by constructing yes/no questions on real-world images with three negative-sampling protocols (*random*, *popular*, *adversarial*); we report all corresponding metrics including accuracy, precision, recall, F1, and the yes-ratio as required by the official script. ScienceQA con-

Math Neuron Ratios: Text vs Vision Models

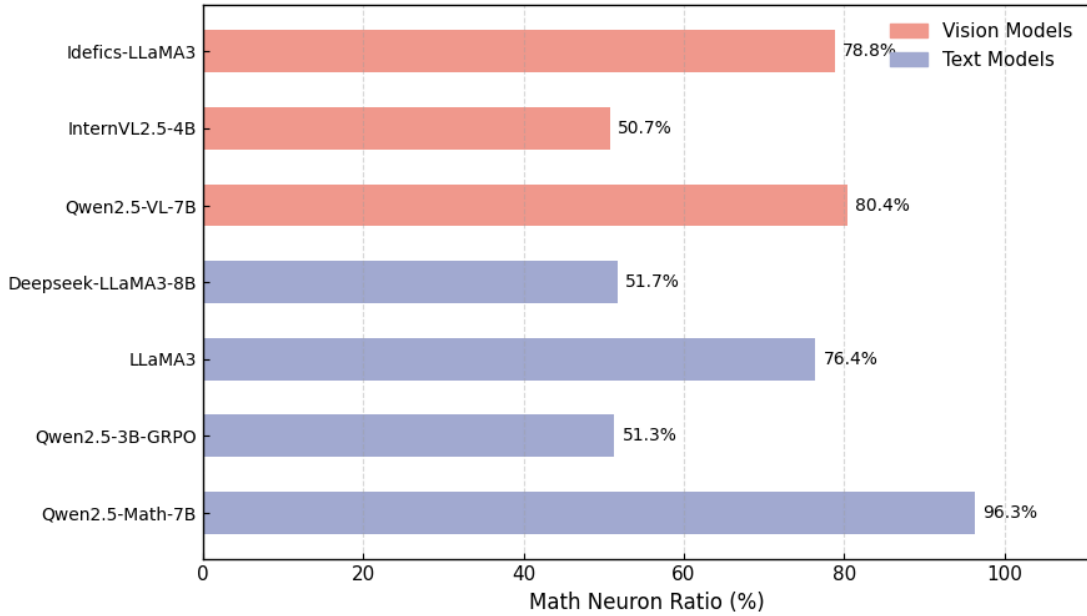


Figure 12. Math neuron ratios across text and vision models. Vision models (red) and text models (blue) are compared by their proportion of math-related neurons, showing that a substantial fraction of shared neurons are activated by mathematical concepts.

Model Name	Params	Vision Encoder / Language Backbone	Merged / Text Backbone	Checkpoint
Idefics3-8B-LLaMA3	8B	SigLip vision + LLaMA3 (8B)	DeepSeek-LLaMA3	HuggingFaceM4/Idefics3-8B-LLaMA3
LLaVA-Next-8B	8B	(vision encoder as used in LLaVA-NeXT) + LLaMA3 (8B)	DeepSeek-LLaMA3	lmms-lab/LLaMA3-LLaVA-Next-8B
Qwen2.5-VL-7B	7B	Qwen2.5 vision + Qwen2.5-VL backbone	Qwen2.5-7B-Math	Qwen/Qwen2.5-VL-7B-Instruct
Intern2.5-VL-4B	4B	InternViT vision + Intern2.5-VL	Qwen2.5-3B-GRPO	OpenGVLab/InternVL2_5-4B
Qwen2.5-3B-Instruct-Math-GRPO	3B	— (text-only model)	Qwen2.5-3B-GRPO	Williammsg/Qwen2.5-3B-Instruct-Math-GRPO

tains multi-choice science questions enriched with lecture notes and human-written explanations. We do not fine-tune on its training set but use the `val` split for prompt development and evaluate on the hidden `test` set, optionally eliciting chain-of-thought inference when explanations are requested.

The original MMMU benchmark covers six major disciplines, more than thirty subjects, and over one hundred and eighty fine-grained sub-fields at college level. It provides `dev`, `val`, and `hidden test` sets and requires submission to an official evaluation server; we use only the public `dev` and `val` data for prompt and parameter tuning and report official `test` scores. MMMU-Pro raises the difficulty with vision-only protocols, stricter filtering of text-answerable questions, and stronger distractor design, offering a more robust evaluation of cross-domain inference.

Inference follows unified prompting. For multiple-choice tasks we instruct the model to output only the letter of the final answer, and for POPE we constrain output to `{yes, no}`. Multi-image questions are fed as ordered

lists with minimal positional hints. Unless chain-of-thought or self-consistency is explicitly required, decoding temperature is set to 0; for CoT we use temperature 0.7 and majority vote over five samples. Metrics are primarily accuracy for MathVista, ScienceQA, MME, MMMU, and MMMU-Pro, with per-subdomain breakdowns where applicable, while POPE additionally reports precision, recall, F1, and yes-ratio. Finally, we respect all dataset licenses and use the data strictly for academic research.